International Journal of Power and Energy Systems, Vol. 43, No. 10, 2023
An Open Access Paper

OPTIMISED QUADRATURE AXIS CURRENT-BASED REGENERATIVE BRAKING OF INDUCTION MOTOR FOR ULTRACAPACITOR-DRIVEN ELECTRICAL VEHICLE

P.K. Athul Vijay, Varsha A. Shah, and Ujjval B. Vyas

Abstract

This article employs the concept of regenerative braking (RB) in induction motor (IM) to extend the range of ultracapacitor (UC)-driven electric vehicles (EVs). Despite its ultra-fast charge–discharge capabilities, UC-driven EV technology is stagnant due to its low energy density, which reduces its range. This article adopts RB technology to extend the range. The high power density and high calendar life of the UC allow maximum capturing of regenerative energy. The paper proposes an optimal torque algorithm to extract maximum regenerative energy from an IM. The motor torque is a function of quadrature current (I_{qs}). The proposed algorithm derived the optimal value of torque by extracting the maximum amount of I_{qs} with respect to variation of motor speed by considering inertia, damping factor, and losses. The indirect FOC control with space vector pulse width modulation and proposed RB algorithm has been utilized for the control of IM. The proposed algorithm has been simulated in MATLAB/Simulink environment and is validated in the OPAL-RT. Results show that energy delivered by the UC without and with conventional, and with the proposed RB algorithm for a 12.83 km run of Tata Nano vehicle model for a standard New York City Cycle schedule is 2077.1 Wh, 1902.5 Wh, and 1671.9 Wh, respectively. The proposed algorithm has achieved 19.5% and 12.12% energy-saving compared to without regenerative and conventional RB.

Key Words

Electrical vehicle, ultracapcitor, regenerative braking, New York city cycle, induction motor

1. Introduction

Electric vehicle (EV) in the transport sector is an effective solution to mitigate the greenhouse gas emission [3]. The usage of EVs has increased drastically over the past decade. The worldwide electric car sales soared to 6.5 million units in 2021. The majority are battery-electric cars, and near 3.5 million unit sales in 2021. By considering the statistics of EV market share of total new car sales between 2013 and 2021 in different countries are shown in Table 1. The statistics show that the EV market has a substantial worldwide growth over the past decade, and it will be more in the further years [16].

EV system is an integration of energy storage devices and electric propulsion. EV requires an energy source characterised by high power and energy densities. The power density determines the maximum acceleration, and energy density determines the range of the EV. However, energy sources with both characteristics are still not commercially available. The commonly utilised batteries are characterised by high energy and lower power densities, while ultracapacitors (UCs) are characterised by high power and lower energy densities [20], [21]. Researchers have tackled this problem by hybridisation of both batteries and UCs in EV. However, hybridising two sources required ample space, a complex control algorithm, additional power electronics circuitry, and sensors [6]. Hence, the EV with a single source is more effective than a hybridised source. At present, batteries are the most commonly used energy source in single-sourced EVs. However, its utilisation in EV results in extensive degradation due to frequent start, stop, acceleration, and deceleration of the vehicle, especially for an urban drive [15]. UC, due to its high power density, large life cycle, high temperature withstands capability, high charge–discharge efficiency, reasonable transient charge, and discharge performance, is emerging as an alternative source to battery in EV [20], [17].

Studies have shown that UC can perform as a primary energy storage device in the EV [17]. The Chinese company Sunwin made an electric bus with the UC as the primary source and have a mileage of 3–6 km, which charge adequately at each bus stop [5]. The present UC technologies have a low energy density that hinders

Department of Electrical Engineering, Sardar Vallabhbhai National Institute of Technology, Surat, India 395007; e-mail: {ds17el008, vas}@eed.svnit.ac.in; ujjvalbvyas@gmail.com
Corresponding author: P.K. Athul Vijay

Recommended by Shuhui Li
(DOI: 10.2316/J.2023.203-0422)

Table 1
EV Market Share of Total New Car Sales between 2013 and 2021 [16]

	2013	2014	2015	2016	2017	2018	2019	2020	2021
Canada	0.181	0.283	0.354	0.582	0.923	2.164	3.01	3.301	3.753
China	0.08	0.23	0.84	1.31	2.12	4.21	4.92	5.42	5.73
Denmark	0.292	0.881	2.29	0.63	0.40	2	4.20	16.20	32.81
France	0.831	0.701	1.191	1.451	1.981	2.12	2.81	11.21	18.12
The Netherlands	5.56	3.88	9.75	6.71	2.61	5.41	14.91	24.61	21.89
India	6.11	13.25	26.46	34.7	55.3	76.91	95.6	109.3	163.6
Iceland	0.941	2.711	3.982	6.281	8.71	19.01	22.61	45.01	53.72
USA	0.621	0.751	0.661	0.901	1.161	1.932	2.01	1.91	3.81
UK	0.161	0.591	1.071	1.251	1.401	1.901	22.601	45.001	50.22

the range of EV [17]. The range can be improved by adopting the concept of regenerative braking (RB). The RB methodology charges the UC by recapturing the inertial energy of rotating components present in the EV during deceleration and braking conditions [19]. It is achieved by reducing the stator magnetic field frequency compared to the frequency of the rotor magnetic field, thereby developing a negative slip. The negative slip implies the increase in the rotor speed compared to the rate of the stator magnetic field, which reverses the relative speed between the stator magnetic field and the rotor conductor. This reversal causes the reversal of the rotor current and hence the stator current. Thus, power flows from the motor to the source. This reverse of the power flow stops when the slip becomes positive during the deceleration of the vehicle. This is avoided by constantly reducing the frequency and voltage of the stator by a scalar or vector control until the motor arrives at a standstill condition during barking. The same concept is also being used during the vehicle's deceleration, effectively increasing the regenerative energy [19].

In the existing studies, academics and industry research worldwide have carried numerous investigations on the RB system (RBS). The RBS has already been commercialized by automotive companies, such as BMW, Toyota, Nissan, Tesla, Mahendra, *etc.,* [24]. Most of the studies on RBS of EVs consider batteries as a source. Very few studies are available in the literature considering UC as a primary source for EV with RBS. In [12], Hinov *et al.* discussed the role of the UC in the RBS, in which the author charged the UC under RBS with different currents and proved that RBS has less impact on UC capacitance degradation. In [4], a UC-based RBS is modelled with a dc-to-dc converter to charge the UC and the author claimed that UC provides an efficient means of storing RB energy. The literature studies have highlighted that plenty of research occurred on both UC and their fundamental properties. However, the drive of EV with UC as a sole energy source with a proper RBS algorithm is rarely discussed.

Most of the studies on RBS primarily focused on the coordination between regenerative and frictional braking. Such as control on the RB force generated by the electric motor and mechanical force caused by the pneumatic or hydraulic brake with series and parallel braking strategies [14]. However, the literature rarely discussed the methodology to achieve RB in an induction motor (IM). Studies showed that efficient RB could be obtained either by controlling the motor torque or the motor flux during the vehicle's deceleration [1], [7]. In [2], the author introduces a ripple correlation control method to identify the optimal value of flux for efficient RB. The author claims that power regeneration with optimal flux is more in comparison with constant flux. However, the studies have proven that speed control of IM during deceleration of the vehicle is difficult to achieve with an optimal flux algorithm [1], [7], [13], [11].

In [23], the RB is considered as a class of parameter uncertain switching systems with external disturbance based on a switched system theory. However, the control algorithm is complex, and the performance of the system under a standard drive schedule remains undiscussed. In [7], Poonam *et al.* formulated optimal RB torque by using a variational method. However, the methodology required prior knowledge about the vehicle's speed at the starting and ending point of the deceleration, which restricts the algorithm utilisation for an unknown drive schedule. In [11], Partridge and Abouelamaimen formulated an RB torque to meet maximum regenerative energy over the entire regenerative period and obtain maximum power return at each braking instant. The methodology utilised the Hamiltonian equation by incorporating the concept of complete energy recuperation. However, the mathematical derivation of formulated regenerative torque remains undiscussed. In [1], Franzò and Nasca developed an optimal value of torque for permanent magnet motor by considering the variation of motor quadrature axis current with respect to motor flux. In it, the motor power input is taken as zero for the formulation of optimal regenerative torque. The studies have shown that the motor's input power

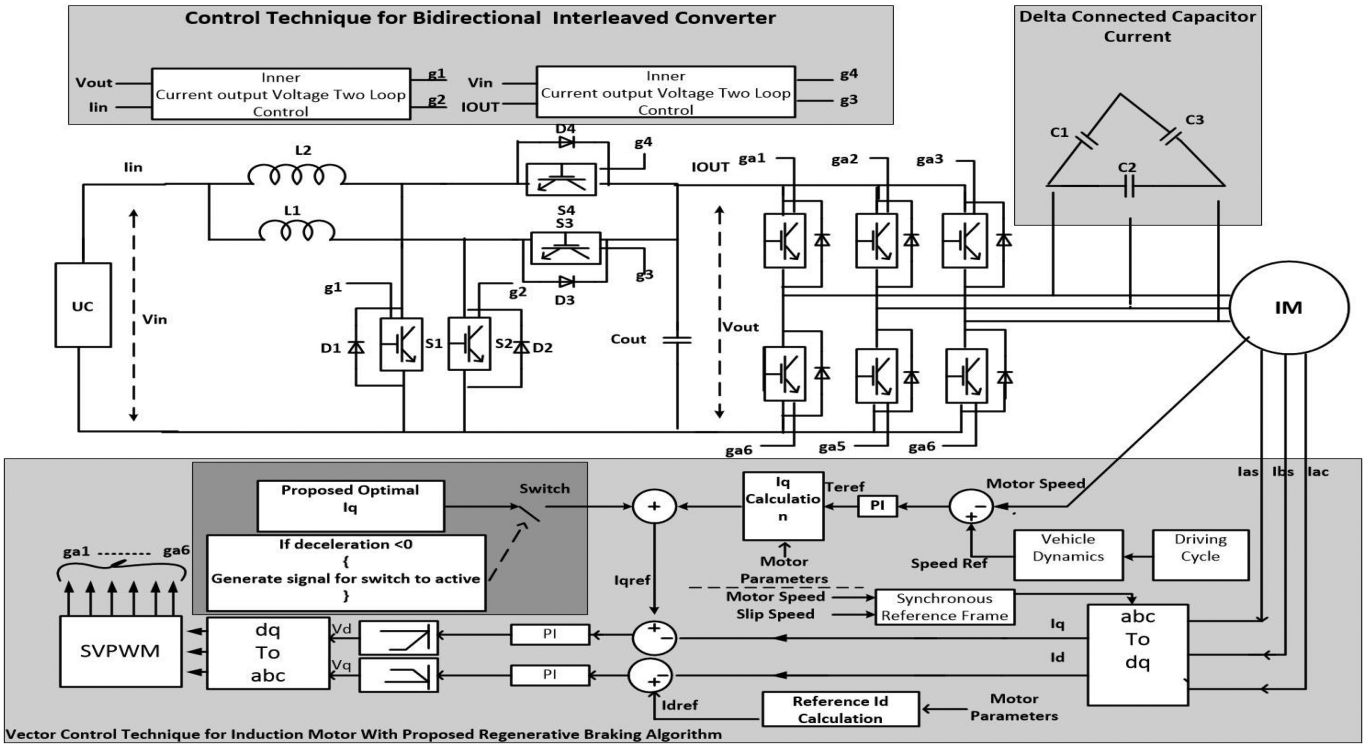

Figure 1. EV system configuration with control techniques.

can be represented by reverse polarity as a function of motor speed, damping factor, and motor inertia during the vehicle's deceleration rather than considering the input power to zero [7]. Also, considering the variation of motor quadrature axis current with respect to the motor speed is more appropriate to formulate the optimal value of regenerative torque in an IM [9]. Hence, this work incorporates the same to develop an optimal regenerative torque for the IM.

The motto of this work is to develop an efficient RB algorithm of IM for an EV with UC as a sole energy storage system, which should be valid for any driving pattern. The proposed algorithm derived the optimal value of torque, which is achieved by extracting the maximum amount of motor quadrature axis current (Iqs) with respect to motor speed variation by considering the motor inertia, damping factor, losses, *etc.* The work utilised an EV model, which comprises a UC as the source, interleaved converter as bidirectional dc-to-dc converter, and an IM drive. Also, a delta-connected capacitor has been included in the system to provide sufficient reactive power to the IM during RB [18]. The content of this paper is to demonstrate the performance of the UC-driven EV under a different operating condition of the driving pattern with a proposed RB algorithm in the constant torque region of the IM. The indirect vector control with space vector pulse width modulation (SVPWM) technique has been utilised along with the RB algorithm for efficient working of the EV model [8], [19]. The work also discussed the total efficiency of motor drive with the proposed RB algorithm of a UC-driven EV for a standard New York City Cycle (NYCC). This paper provides an effective solution for the low mileage issues of UC-driven EVs. The required power and torque to drive the vehicle has been calculated by considering all the vehicles dynamics [19] of Tata Nano.

2. EV System under Consideration with Control Technique

The UC-driven EV has a UC connected to the interleaved bidirectional converter to maintain the constant dc bus voltage. The IM drive is controlled through a six switch dc-to-ac converter operated through the SVPWM technique. The speed/torque of IM is controlled through field-oriented control (FOC) in the synchronously rotating reference frame [9], [19]. The input into the FOC algorithm comprises stator current, rotor speed of IM, and reference speed from the standard driving cycle. The required power and torque to drive the vehicle have been calculated by considering all the vehicle's dynamics. During the deceleration and stopping of the vehicle, the FOC control algorithm is modified with the proposed algorithm for devising reference current in the quadrature axis (Iqs) towards the negative direction for efficient RB. The entire algorithm is designed to work in the variable power region of IM. The delta-connected capacitor bank has been utilised to supply sufficient reactive power to the induction machine during the regenerative period [18]. The same has been shown in Fig. 1.

3. Proposed Control Algorithm for Regenerative Braking of IM

Mathematical representation of the *dq* model of the IM can be represented as shown in (1).

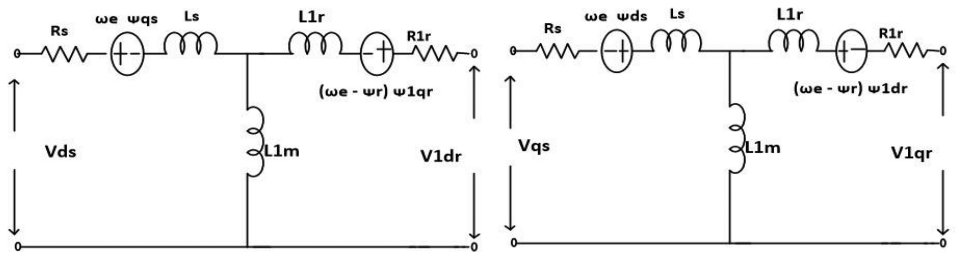

Figure 2. dq equivalent model of IM.

$$\begin{bmatrix} V_{ds} \\ V_{qs} \\ V_{dr}^1 \\ V_{qr}^1 \end{bmatrix} = \begin{bmatrix} r_s + \frac{d}{dt}L_s\sigma & \omega_e\sigma L_s & \frac{L_m^1}{L_r^1}\frac{d}{dt} & \frac{\omega_e L_m^1}{L_r^1} \\ -\omega_e\sigma L_s & r_s + \frac{d}{dt}L_s\sigma & -\frac{\omega_e L_m^1}{L_r^1} & \frac{L_m^1}{L_r^1} \\ \frac{-r_r^1 L_m^1}{L_r^1} & 0 & \frac{r_r^1}{L_r^1} + \frac{d}{dt} & (\omega_e - \omega_r) \\ 0 & -\frac{L_m^1}{L_r^1} & -(\omega_e - \omega_r) & \frac{r_r^1}{L_r^1} + \frac{d}{dt} \end{bmatrix} \begin{bmatrix} I_{ds} \\ I_{qs} \\ \psi_{dr}^1 \\ \psi_{qr}^1 \end{bmatrix} \tag{1}$$

The V_{ds}, V_{qs}, V'_{dr}, V'_{qr}, Lr, L'_r, and $L'_m$are the d-axis stator voltage and q-axis stator voltage, d-axis rotor voltage referred to the primary side, q-axis rotor voltage referred to the primary side, stator inductance, rotor inductance referred to the primary side, and mutual inductance referred to the primary side, respectively, as shown in Fig. 2.

The d–q axis voltage in the stator and rotor can be represented in terms of d–q axis current and flux linkage in rotor and stator, respectively. Where ψ'_{dr} and ψ'_{qr} are the stator and flux linkage in rotor d- and q-axis is referred to the primary side (stator) [9].

$$L_m^1 = \frac{N_s}{N_r}L_m, L_r^1 = \left(\frac{N_s}{N_r}\right)^2 L_r, r_r^1 = \left(\frac{N_s}{N_r}\right)^2 r_r \tag{2}$$

N_s and N_r are the number of turns in the rotor and the stator [9].

$$\psi_{ds} = L_s I_{ds} + L'_m I'_{dr}, \psi_{qs} = L_s I_{qs} + L'_m I'_{dr} \tag{3}$$
$$\psi'_{dr} = L'_r I'_{dr} + L'_m I'_{ds}, \psi'_{qr} = L'_r I'_{qr} + L'_m I'_{qs}, \tag{4}$$

ψ_{ds} and the ψ_{qs} are the flux linkages in the stator and rotor side. From the motor power equations, the electromagnetic torque developed by the motor can be represented as shown in (5) [9].

$$T_e = \frac{3}{2}\frac{P}{2}L'_m(I_{qs}I'_{dr} - I_{ds}I'_{qr}) \tag{5}$$

With the vector control, the net flux can be aligned into the d-axis and net torque in the q-axis. Hence, T_e is modified as shown in (6) [9].

$$T_e = \frac{3}{2}\frac{P}{2}\frac{L_m}{L_r}(I_{qs}\psi_{dr}) \tag{6}$$

The optimal value of the torque can be obtained by either optimising motor quadrature axis current I_{qs} or by optimising ψ_{dr}. However, the induction machine is operating in the constant torque region, hence, the flux ψ_{dr} remains constant. The optimal value of I_{qs} can be derived as shown in (7)–(19).

$$P_{in} = P_{em} + P_{\text{loss}} \tag{7}$$

P_{in} is the power input to the IM. P_{em} is the power developed in the motor and P_{loss} is the losses in the IM. During the normal acceleration and the constant speed operation of the IM, P_{in} is the summation of P_{em} and P_{loss} as shown in (7). During the RB, active power is from the induction machine. Hence, the power balance equations during the deceleration or stopping of the vehicle can be modified as shown in (8).

$$-P_{in} = P_{em} + P_{\text{loss}} \tag{8}$$

Power output $(-P_{in})$ from the IM can be represented in terms of the moment of inertia (j) and damping factor (ζ) as shown in (9) [7].

$$P_{in} = J\frac{d\omega_{rm}}{dt}\omega_{rm} + \zeta\omega_{rm}^2 \tag{9}$$

ω_{rm} is the motor rotor speed in rad/s. P_{em} can be represented in terms of the T_{em} and ω_{rm} as shown in (10).

$$P_{em} = \frac{3}{2}\frac{P}{2}\frac{L_m}{L_r}I_{qs}\psi_{dr}\omega_{rm} \tag{10}$$

Losses in the IM can be represented in terms of the total resistance of the IM in the stator and rotor (R) and motor d- and q-axis current as shown in (11)–(13)

$$P_{loss} = R[I_{ds}^2 + I_{qs}^2] \tag{11}$$
$$R = R_s + R'_r \tag{12}$$

Where R_s and R_r are the motor stator and rotor resistance.

$$R = R_s + R'_r = R_s + \left(\frac{N_s}{N_r}\right)^2 R_r \tag{13}$$

Substituting (9), (10), and (11) into (8) results in a quadratic equation in terms of I_{qs} as shown in (14)

$$I_{qs}^2 R + \frac{3}{2}\frac{P}{2}\frac{L_m}{L_r}I_{qs}\psi_{dr}\omega_{rm} + \left(J\frac{d\omega_{rm}}{dt}\omega_{rm} + \zeta\omega_{rm}^2 + RI_{ds}^2\right) = 0 \tag{14}$$

Equation (14) gives a quadratic equation. The solution of I_{qs} is shown in (15)

$$I_{qs} = \frac{-A\omega_{rm} + \sqrt{(A\omega_{rm})^2 - 4R\left(J\frac{d\omega_{rm}}{dt}\omega_{rm} + \zeta\omega_{rm}^2 + RI_{ds}^2\right)}}{2R} \tag{15}$$

Equation (15) describes the motor q-axis current I_{qs} in the RB region. Substituting the obtained I_{qs} in (15) describes the motor torque in the RB region.

$$A = \frac{3}{2}\frac{P}{2}\frac{L_m}{L_r}\psi_{\mathrm{dr}} \tag{16}$$

By finding the derivative of I_{qs} with respect to ω_{rm} (17) and equating into zero (18) will provide an optimal value of quadrature axis current (I_{qoptimal}) to extract maximum energy during the deceleration or stopping of the vehicle (19).

$$\frac{dI_{\mathrm{qs}}}{d_{\omega_{\mathrm{rm}}}} = \frac{1}{2R} \left(-A + \frac{2A^2\omega_{\mathrm{rm}} - 4R\left(2\zeta\omega_{\mathrm{rm}} + j\left(\omega_{\mathrm{rm}}\frac{d^2\omega_{\mathrm{rm}}}{\mathrm{dtd}\omega_{\mathrm{rm}}} + \frac{d\omega_{\mathrm{rm}}}{\mathrm{dt}}\right)\right)}{2\sqrt{A^2\omega_{\mathrm{rm}}^2 - 4R\left(J\frac{d\omega_{\mathrm{rm}}}{\mathrm{dt}}\omega_{\mathrm{rm}} + \zeta\omega_{\mathrm{rm}}^2 + RI_d^2\right)}}\right) \tag{17}$$

Applying the boundary conditions.

$$\frac{dI_{\mathrm{qs}}}{d\omega_{\mathrm{rm}}} = 0 \tag{18}$$

$$I_{\mathrm{qoptimal}} = \frac{1}{2R}(-A\omega_{\mathrm{rm}} + \frac{1}{2A}(2A^2\omega_{\mathrm{rm}} - 4R\left(2\zeta\omega_{\mathrm{rm}} + j\left(\omega_{\mathrm{rm}}\frac{d^2\omega_{\mathrm{rm}}}{\mathrm{dtd}\omega_{\mathrm{rm}}} + \frac{d\omega_{\mathrm{rm}}}{\mathrm{dt}}\right)\right) \tag{19}$$

Substituting I_{qoptimal} into (6) will result in an optimal value of regenerative torque for regenerative period of the vehicle.

$$T_{\mathrm{optimal}} = \frac{1}{2R}(-A^2\omega_{\mathrm{rm}} + \frac{1}{2}(2A^2\omega_{\mathrm{rm}} - 4R\left(2\zeta\omega_{\mathrm{rm}} + j\left(\omega_{\mathrm{rm}}\frac{d^2\omega_{\mathrm{rm}}}{\mathrm{dtd}\omega_{\mathrm{rm}}} + \frac{d\omega_{\mathrm{rm}}}{\mathrm{dt}}\right)\right) \tag{20}$$

4. Simulation Studies and Discussion

The simulation studies have been carried out with the system as shown in Fig. 1. The EV system with the proposed RB algorithm is simulated in MATLAB/Simulink with two different driving schedules. First with a random drive cycle (for 1 km run), and the second is with the standard NYCC for a 12.83 km. The Tata Nano four-wheeler is selected as the vehicle model. The gear ratio of 4:1 has been utilised in this work.

4.1 Performance of the UC-driven EV model for a Random Drive Schedule with the Proposed Regenerative Braking Algorithm

To test the performance of the proposed RB algorithm, initially run the vehicle model for a random drive schedule of 1 km. Figure 3 shows the speed (RPM), torque characteristic of the IM, output voltage of bidirectional interleaved dc-to-dc converter, the terminal voltage of UC, and source current for a random drive cycle. For the entire drive range, the speed of the IM shows an excellent tracking of the reference speed provided through the driving cycle. During the acceleration and constant speed profile, the dc bus voltage remains constant at

Table 2
Vehicle Specification

Sl.no	Vehicle Parameter	Specifications
1	Vehicle and passenger mass	1005 kg
2	Mass factor (f_m)	1.05
3	Coefficient of rolling resistance (C_{rr})	0.02
4	Air density (ρ)	1.225 kg/m^3
5	Coefficient of drag (C_d)	0.5
6	Wind speed	1.39 m/s
7	Road slope	0°
8	Frontal area of car (A_f)	2.45 m^2

Table 3
IM Specification

Sl.no	Motor Parameter	Specifications
1	Power	5 kW
2	Voltage	415(L) V
3	Mutual inductance (L_m)	34.7 mH
4	Pole and frequency	4 and 50 Hz
5	Self inductance (L_s)	0.8 mH
6	Rotor inductance (L_r)	0.8 mH
7	Stator resistance (R_s)	0.0827 Ω
8	Rotor Resistance (R_r)	0.0228 Ω

Table 4
UC Specification

Sl.no	Parameter	Specifications
1	Capacitance	187.5 F
2	Equivalent series resistance (ESR)	7.8 mΩ
3	Number of series cell	112
4	Number of parallel cell	7
5	Total discharge time	900 s
6	Rated voltage	300 V

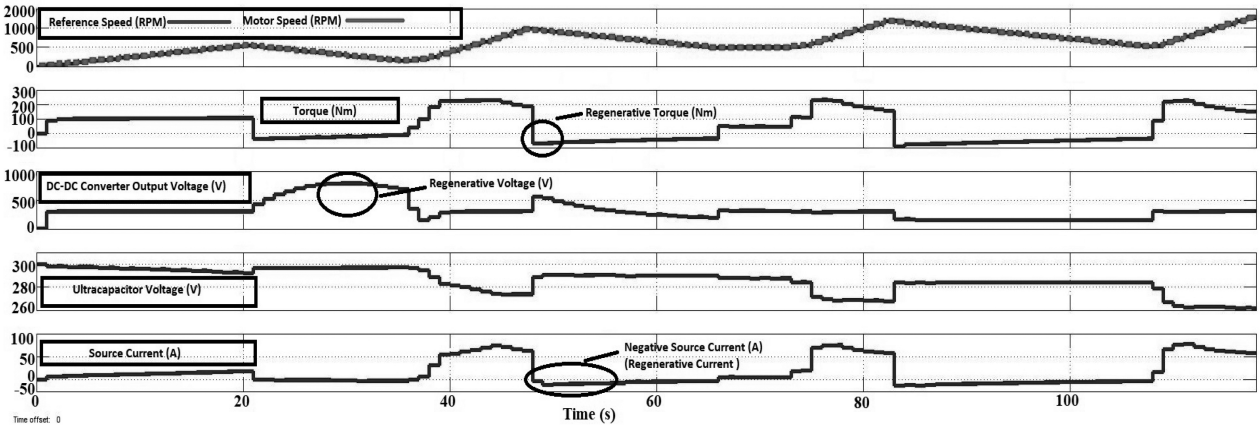

Figure 3. Performance of electrical vehicle under different dynamic conditions.

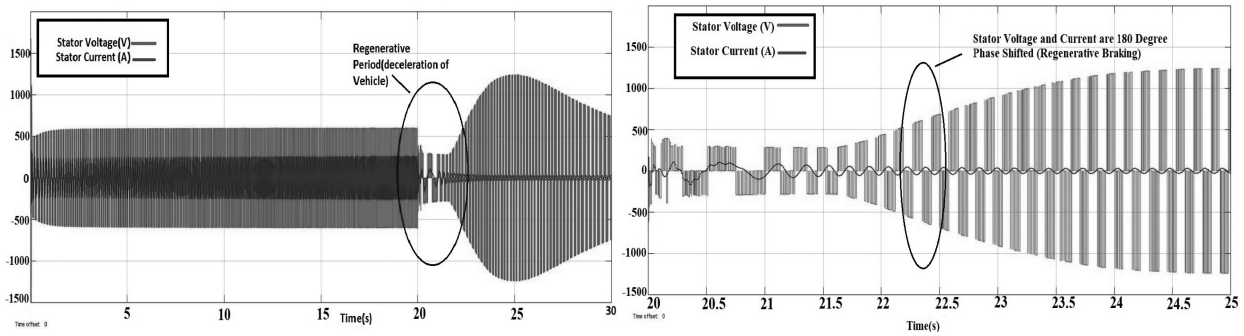

(a) (b)

Figure 4. (a) Stator voltage and current of IM. (b) Enlarged stator voltage and current of IM.

Table 5
Interleaved Converter Specification

Sl.no	Parameters	Specifications
1	Low side voltage (V_L)	300 V
2	High side voltage (V_H)	600 V
3	Output capacitance (C_{out})	0.0090 F
4	Input inductor (L_1)	21×10^{-4} F
5	Input inductor (L_2)	21×10^{-4} F
6	Switching frequency (f_s)	10 kHz

600 V, and the source current remains positive. During the deceleration, the source current, motor torque achieved a negative value. Also, increment in the dc bus voltage and the terminal voltage of the UC (RB). Figure 4 shows the IM stator voltage and the stator current for the random driving schedule. During the acceleration and constant speed operation of IM, the stator voltage and current of the IM remain about in phase to each other (phase angle between the stator voltage and stator current will be dependent on the reactive power required by the IM). During the RB of the IM, the stator voltage and current of the IM remains 180° out of phase.

4.2 Performance of the EV model for an NYCC with the Proposed Regenerative Braking Algorithm

To validate the performance of the proposed algorithm, the EV model runs for an NYCC schedule of 12.83 km. Figure 5 shows the speed (RPM), torque characteristics of the IM, output voltage of the bidirectional interleaved dc-to-dc converter, the terminal voltage of UC, and source current. For the entire drive range, the speed of IM shows an excellent tracking of the reference speed provided through the driving cycle. Also, the system employees efficient RB (negative source current and negative electromagnetic torque).

The electromagnetic torque of IM for a driving range of 12.83 km with the NYCC schedule has been shown in Fig. 6(a). Since the load is a vehicle load with a variable speed profile, IM's electromagnetic torque is dynamic. Also, the UC (source) has steep droop voltage characteristics with the drain of energy. But with the assist of a dc/dc converter, the dc bus voltage will remain constant during acceleration and the constant speed profile of the vehicle. However, the results have shown that the dynamic nature of UC voltage and the vehicle load produce torque ripples. The peak-to-peak torque ripples of IM for the same driving range has been observed in the field of 1 to 2 Nm as shown in Fig. 6(b).

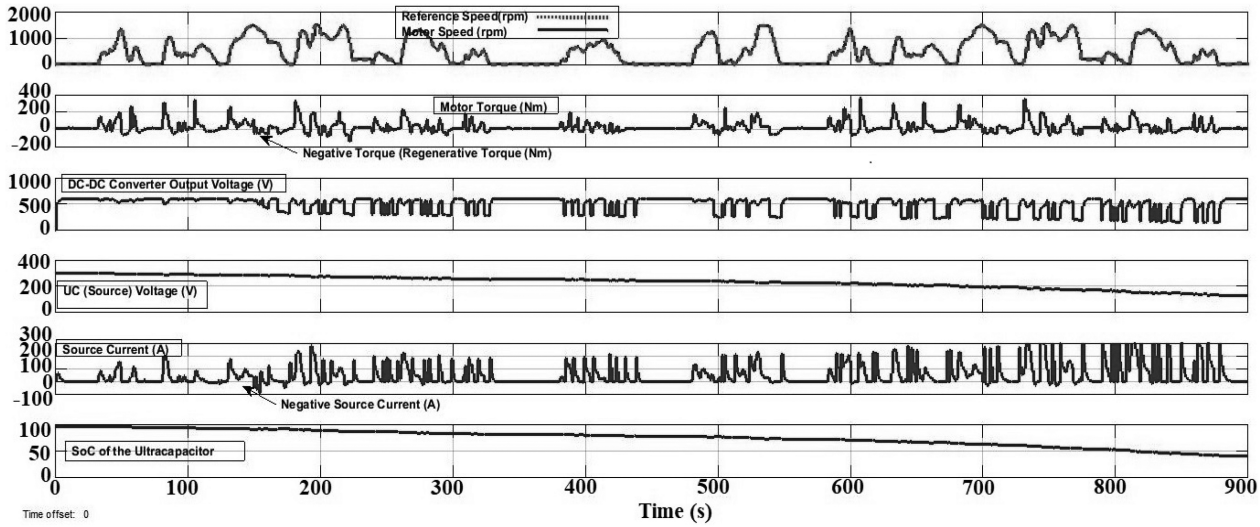

Figure 5. Performance of the EV with an NYCC.

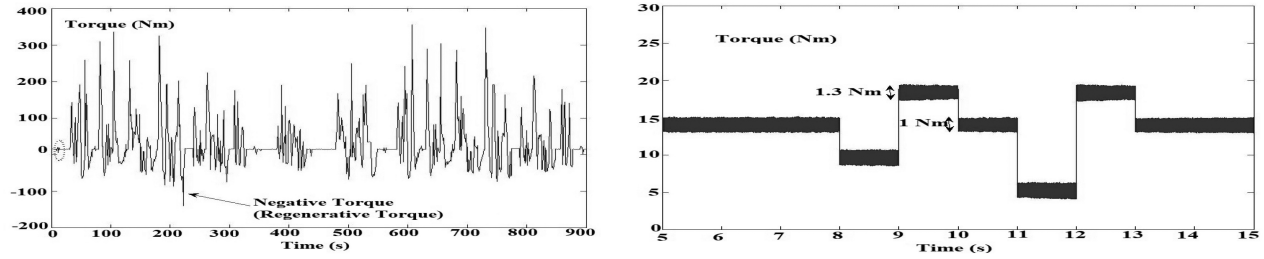

(a) (b)

Figure 6. Electro magnetic torque of IM for an NYCC drive of EV. (a) Motor torque for NYCC drive. (b) Enlarged motor torque for NYCC drive.

4.3 Efficiency Model of IM Drive

Losses in the IM comprise of stator and rotor copper losses, stray loss, core loss, and friction/windage losses. To compute aggregate IM losses, it is acute to identify the stator current (I_s), rotor current (I_r), and the airgap voltage (V_g) as shown in (21), (22), and (23) [22]. In order to derive the same, the per phase equivalent circuit of IM is refereed as shown in Fig. 2.

$$I_r = \sqrt{\frac{2}{3}\frac{T_e\omega_e}{P}\frac{S}{R_r^1}} \tag{21}$$

$$I_s = I_r\frac{\sqrt{\left(\frac{R_oR_r'}{S}-\omega_e^2L_r'L_o\right)^2+\left(\omega_e(R_oL_o+\frac{R_r^1L_o}{S}+R_oL_r')\right)^2}}{R_o\omega_eL_o} \tag{22}$$

$$V_g = \sqrt{\frac{S\omega_eT_e}{3R_r'}\left(\frac{R_r'}{S^2}+\omega^2{L_r'}^2\right)} \tag{23}$$

Total power loss in the IM can be represented as shown in Fig. 24.

$$P_{m-\text{loss}} = 3[I_S^2R_s + I_r^2R_r' + \frac{V_g^2}{R_o}] \tag{24}$$

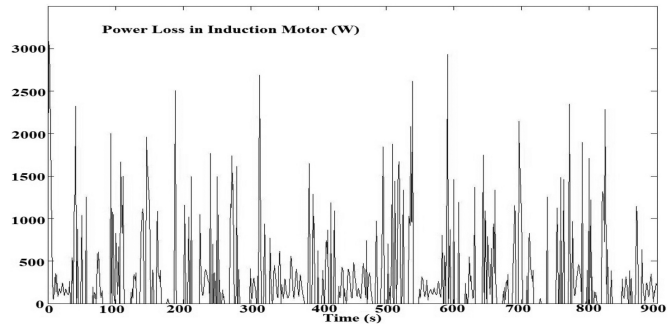

Figure 7. Total power loss in IM drive.

The primary losses in the inverters are switching and conduction losses. Conduction losses in the inverter comprise of conduction losses of the switch ($P_{\text{cond,sw}}$) and diode($P_{\text{cond},D}$). Switching losses in the inverter comprise of switching losses of the switch ($P_{\text{sw},D}$) and diode ($P_{\text{sw,sw}}$) [22].

$$P_{\text{loss,inv}} = 6*(P_{\text{cond,sw}}+P_{\text{cond},D}+P_{\text{sw},D}+P_{\text{sw,sw}}) \tag{25}$$

The average power loss of IM drive for a driving range of 12.83 km of the NYCC drive schedule is 310.57 watts, as

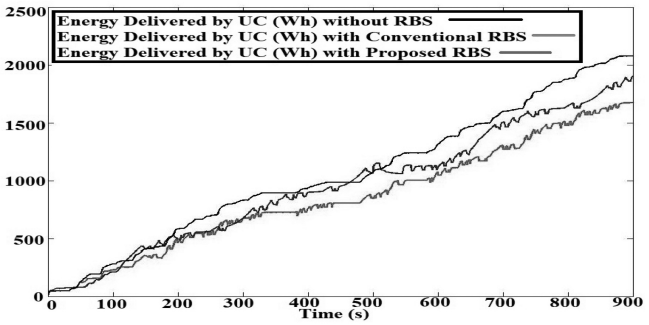

Figure 8. Energy delivered by UC.

Table 6
Energy Consumption by EV

	Energy Delivered By the UC	Energy Saving	Mileage Saving
Without regenerative braking (WRB)	2077.1 Wh	0	0
With conventional regenerative braking (WCRB)	1902.5 Wh	8.4%	≈1.1 km
With proposed regenerative braking (WPRB)	1671.9 Wh	19.5%	≈3 km

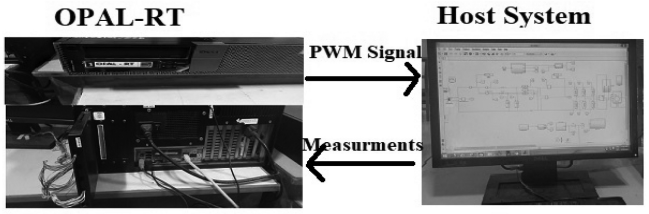

Figure 9. RT LAB test bench.

shown in Fig. 7. The average power input to the motor for the same running range is 2719.46 watts. Hence, the total average efficiency of an IM for an entire driving range is 88.6%.

Figure 8 shows the energy delivered by the UC for an NYCC drive of 12.83 km with no RB algorithm, with the conventional RB algorithm, and with the proposed RB algorithm.

Table 6 shows the energy consumption by simulated UC-driven EV model for a UDDC without, with conventional, and with proposed RB algorithms, respectively.

4.4 Validation of Algorithm Using OPAL-RT

The work has utilised an OPAL-RT electric hardware solver (eHS) to demonstrate the real-time simulation. The test bench for real-time simulation has been shown in Fig. 9, which comprises an HOST system (PC) for the

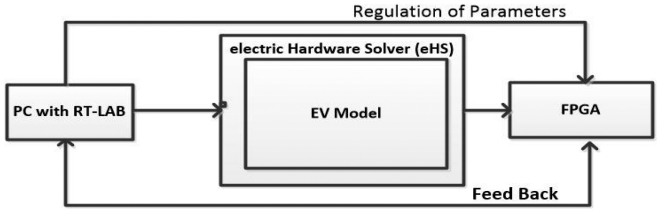

Figure 10. Flow of eHS in RT LAB.

development of power and control circuitry and field-programmable gate array FPGA-based OPAL-RT system for the real-time implementation of the system. The eHS solver is an FPGA-based technology developed by OPAL-RT for real-time power electronics simulation. The control and power circuits have been made in the MATLAB software and fed to the RT LAB via the eHS solver. The eHS solver uses modified nodal analysis. It solves a conductance matrix to find the voltage at each node of the circuit and the current in each branch. The eHS provides a convenient user interface enabling users to create real-time models created in the simulation tool. The signal from the eHS solver is fed to the FPGA. FPGAs are programmable silicon chips with a collection of programmable logic blocks encircled by input/output blocks that are put unitedly through programmable interconnect resources. The FPGA outputs the gate pulses for the three-phase inverter and the dc/dc converter [10]. The output is fed to the MATLAB workspace and plotted in MATLAB as shown in Figs. 10 and 11.

The proposed algorithm has been tested in real-time simulation for a driving pattern, as shown in Fig. 12, which comprises acceleration and deceleration. The proposed RB algorithm makes motor as a generator during the vehicle deceleration, which is possible by a proper negative electromagnetic torque (negative is a mathematical notation), generated via the proposed RB algorithm as shown in Fig. 15. Once the motor starts acting as a generator, the generated voltage from the induction machine accumulates in the dc bus, as shown in Fig. 14. Depending on the SoC of the UC and DC bus voltage, the current is injected into the UC via dc-to-dc converter (current in the negative direction) as shown in Fig. 13, which implies the successful implementation of the proposed RB for UC-driven IM drive.

5. Conclusion

In this paper, an optimal RB algorithm for the UC-driven EV has been proposed. The algorithm has been simulated with the NYCC drive cycle with MATLAB simulation and validated in the real-time RT Lab simulator. The results show that the energy delivered by the UC without, with conventional, and with proposed RB are 2077.1 Wh, 1902.5 Wh, and 1671.9 Wh, respectively. Energy-saving of 19.5% and 12.12% with mileage saving of approximately 3 km and 1.5 km has been achieved with the proposed algorithm comparison without RB and conventional RB for a 12.83 km run of the Tata Nano vehicle model. Also, for the entire driving range, the efficiency of the IM is 88.6%. Based on

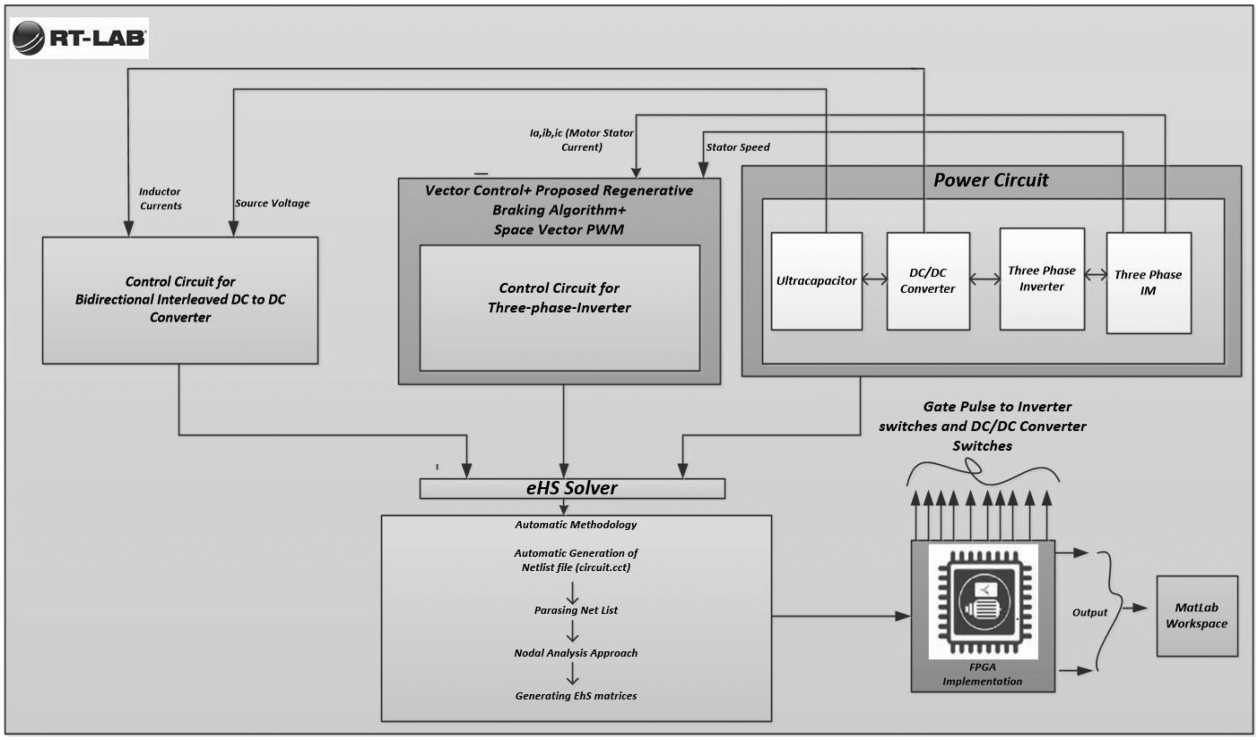

Figure 11. Interfacing diagram of OPAL-RT with MATLAB EV model [10].

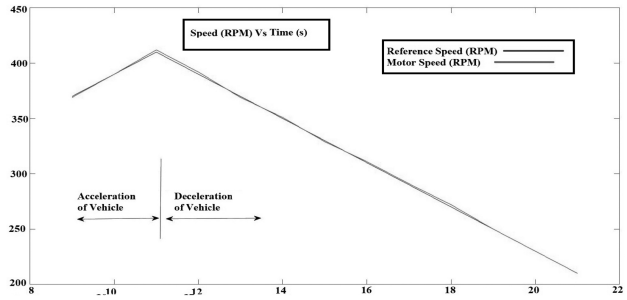

Figure 12. Reference and motor speed in OPAL-RT.

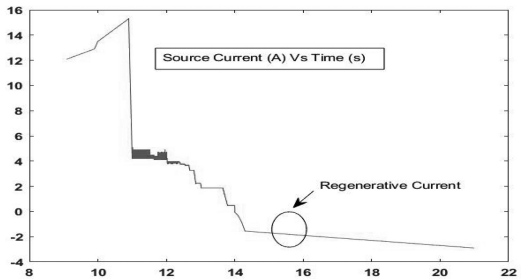

Figure 13. Source (UC) current in OPAL-RT.

this analysis, it can be concluded that UC can be utilised as the sole energy device for a city drive with a proper RB algorithm. This paper provides an effective solution for the low mileage issues of UC-driven EVs.

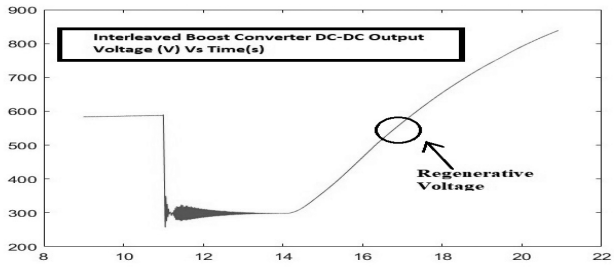

Figure 14. DC/DC converter output voltage in OPAL-RT.

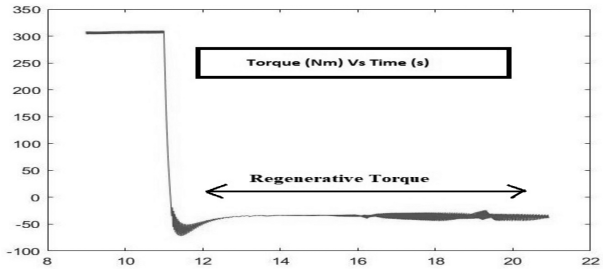

Figure 15. Motor torque in OPAL-RT.

References

[1] S. Franzò and A. Nasca, The environmental impact of electric vehicles: A novel life cycle-based evaluation framework and its applications to multi-country scenarios, *Journal of Cleaner Production*, *315*, 2021, 128005.

[2] J.A. Sanguesa, V. Torres-Sanz, P. Garrido, F.J. Martinez, and J.M. Marquez-Barja, A review on electric vehicles: Technologies and challenges, *Smart Cities*, *4*(1), 2021, 372–404.

[3] P.A. Vijay, V.A. Shah, and V. Shimin, Energy based equivalent circuit modelling of ultracapacitor considering variation of

ESR with OCV, *International Journal of Power and Energy Systems*, *40*(2), 2020, 79–85.
[4] U.B. Vyas, V.A. Shah, A.V. PK, and N.R. Patel, Gaussian exponential regression method for modeling open circuit voltage of lithium-ion battery as a function of state of charge, *COMPEL-The International Journal for Computation and Mathematics in Electrical and Electronic Engineering*, *41*(1), 2021, 64–80.
[5] A. Ibrahim and F. Jiang, The electric vehicle energy management: An overview of the energy system and related modeling and simulation, *Renewable and Sustainable Energy Reviews*, *144*, 2021, 111049.
[6] E. Redondo-Iglesias, P. Venet, and S. Pelissier, Calendar and cycling ageing combination of batteries in electric vehicles, *Microelectronics Reliability*, *88*, 2018, 1212–1215.
[7] Poonam, K. Sharma, A. Arora, and S.K. Tripathi, Review of supercapacitors: Materials and devices, *Journal of Energy Storage*, *21*, 2019, 801–825.
[8] A. Hnatov, S. Arhun, O. Ulyanets, and S. Ponikarovska, Ultracapacitors electrobus for urban transport, *Proc. IEEE 38th Int. Conf. on Electronics and Nanotechnology (ELNANO)*, Kyiv, 2018, 539–543.
[9] V.S. Sudhakaran, V.A. Shah, and M.M. Lokhande, Vector control based regenerative braking for induction motor driven battery electric vehicles, *International Journal of Power and Energy Systems*, *40*(3), 2020, 112–120.
[10] Regenerative braking system market size, share, growth [2029], https://www.fortunebusinessinsights.com/enquiry/request-sample-pdf/automotive-regenerative-braking-system-market-102236.
[11] J. Partridge and D.I. Abouelamaimen, The role of supercapacitors in regenerative braking systems, *Energies*, *12*(14), 2019, 2683.
[12] N.L. Hinov, D.N. Penev, and G.I. Vacheva, Ultra capacitors charging by regenerative braking in electric vehicles, *Proc. 25th Int. Scientific Conf. Electronics (ET)*, Sozopol, 2016, 1–4.
[13] C. Qiu and G. Wang, New evaluation methodology of regenerative braking contribution to energy efficiency improvement of electric vehicles, *Energy Conversion and Management*, *119*, 2016, 389–398.
[14] A. Adib and R. Dhaouadi, Performance analysis of regenerative braking in permanent magnet synchronous motor drives, *Advances in Science, Technology and Engineering Systems Journal*, *3*(1), 2018, 460–466.
[15] K. Inoue, K. Ogata, and T. Kato, Efficient power regeneration and drive of an induction motor by means of optimal torque derived by the variational method, *Journal Electrical Engineering Japan*, *173*(1), 2010, 41–50.
[16] S. Choi, A.M. Bazzi, and P.T. Krein, Ripple correlation control applied to electric vehicle regenerative braking, *Proc. Power and Energy Conf. at Illinois (PECI)*, Urbana, 2010, 88–92.
[17] R.M. Prasad and M.A. Mulla, Direct torque control of rotor-tied DFIG without rotor position sensor, *International Journal of Electrical Power and Energy Systems*, *40*(1), 2020, 29–35.
[18] A.S. Murthy, D.P. Magee, and D.G. Taylor, Optimized regenerative braking of induction machines with indirect field-oriented control, *Proc. IEEE Transportation Electrification Conf. and Expo (ITEC)*, Dearborn, MI, 2016, 1–6.
[19] J. Xie, B. Cao, H. Zhang, and D. Xu, Switched robust control of regenerative braking of electric vehicles, *Proc. IEEE Int. Conf. Information and Automation*, Harbin, 2010, 1609–1612.
[20] P.C. Krause, O. Wasynczuk, S.D. Sudhoff, and S.D. Pekarek, *Analysis of electric machinery and drive systems,* vol. 75. (Hoboken, NJ: Wiley, 2013).
[21] E. O. Silva, W. E. Vano, and G.C. Guimares, Capacitor bank sizing for squirrel cage induction generators operating in distributed systems, *IEEE Access, 8*, 2020, 27507–27515.
[22] P. Jayal and G. Bhuvaneswari, Reduced switching analysis-based space vector modulation algorithm for multilevel inverters, *International Journal of Electrical Power and Energy Systems, 39*(2), 2019, 64–76.
[23] S.S. Williamson, A. Emadi, and K. Rajashekara, Comprehensive efficiency modeling of electric traction motor drives for hybrid electric vehicle propulsion applications, *IEEE Transactions on Vehicular Technology, 56*(4), 2007, 1561–1572.
[24] Z. Li, J. Xu, K. Wang, G. Li, and P. Wu, A discrete small-step synthesis real-time simulation method for power converters, *IEEE Transactions on Industrial Electronics*, *69*(4), 2021, 3667–3676.

Biographies

P.K. Athul Vijay was born in Calicut, India. He received the B.Tech. degree in electrical and electronics engineering from Calicut University, Kerala, India, in 2014, the M.Tech. degree in electrical engineering from Sardar Vallabhbhai National Institute of Technology, Gujarat, India, in 2017, where he is currently pursuing the Ph.D. degree with the Department of Electrical Engineering. His research activity is related to application of power electronics in electric vehicles, ultracapacitor, and induction motor drives.

Varsha A. Shah was born in Surat, India. She received the B.E. degree in electrical engineering from Maharaja Sayajirao University, Gujarat, India, in 1986, the M.E. degree in electrical engineering from Veer Narmad South Gujarat University, Gujarat, India, in 1990, and the Ph.D. degree in electrical engineering from Sardar Vallabhbhai National Institute of Technology, Gujarat, India, in 2013. She has been working as a Professor with the Department of Electrical Engineering, Sardar Vallabhbhai National Institute of Technology, Gujarat, India, since 1987. Her research activity is related to hybrid electric vehicles, smart grid, and power quality issues.

Ujjval B. Vyas received the B.Tech. degree in electrical and electronics engineering from JNTU Ananthapur University, Ananthapuram, India, in 2015, and the M.Tech. degree in power electronics from R V College of Engineering, Bangalore, India, in 2018. He is currently pursuing the Ph.D. degree with the Department of Electrical Engineering, Sardar Vallabhbhai National Institute of Technology, Gujarat, India. His research interest includes battery modelling, battery management system, fast charging strategy, and power electronics application in electric vehicles.